Published in Environmental science & technology 40, 5, 1588-1596, 2006
which should be used for any reference to this work

Does the Rayleigh Equation Apply to Evaluate Field Isotope Data in Contaminant Hydrogeology?

YUMIKO ABE AND DANIEL HUNKELER*
Centre for Hydrogeology, University of Neuchâtel, Rue Emile Argand 11, CH-2009 Neuchâtel, Switzerland

Stable isotope data have been increasingly used to assess in situ biodegradation of organic contaminants in groundwater. The data are usually evaluated using the Rayleigh equation to evaluate whether isotope data follow a Rayleigh trend, to calculate the extent of contaminant biodegradation, or to estimate first-order rate constants. However, the Rayleigh equation was developed for homogeneous systems while in the subsurface, contaminants can migrate at different velocities due to physical heterogeneity. This paper presents a method to quantify the systematic effect that is introduced by applying the Rayleigh equation to field isotope data. For this purpose, the travel time distribution between source and sampling point is characterized by an analytical solution to the advection−dispersion equation. The systematic effect was evaluated as a function of the magnitude of physical heterogeneity, geometry of the contaminant plume, and degree of biodegradation. Results revealed that the systematic effect always leads to an underestimation of the actual values of isotope enrichment factors, the extent of biodegradation, or first-order rate constants, especially in the dispersion-dominant region representing a higher degree of physical heterogeneity. A substantial systematic effect occurs especially for the quantification of first-order rate constants (up to 50% underestimation of actual rate) while it is relatively small for quantification of the extent of biodegradation (<5% underestimation of actual degree of biodegradation). The magnitude of the systematic effect is in the same range as the uncertainty due to uncertainty of the analytical data, of the isotope enrichment factor, and the average travel time.

Introduction

Compound-specific isotope analysis has been increasingly used to assess natural attenuation of organic compounds at contaminated sites. Isotope analysis has been used to investigate sites contaminated with BTEX compounds (*1*−*8*), methyl *tert*-butyl ether (MTBE) (*9*, *10*), and chlorinated hydrocarbons (*11*−*15*). These studies demonstrated a trend of increasing carbon (or hydrogen) isotope ratios of contaminants accompanied by decreasing concentrations because responsible microbial communities preferably consume the molecules with lighter isotopes. Physical factors, such as dispersion, sorption, and evaporation, are generally assumed to have an insignificant influence on isotope ratios (*16*), although a recent study suggests sorption-induced isotope fractionation (*17*). Under certain conditions, sorption may lead to isotopic enrichment at the fringe of expanding plumes, although the effect has not yet been demonstrated at the field scale (*17*). Isotope fractionation is usually quantified by the Rayleigh equation which relates the normalized isotope ratio and the normalized residual concentration by an isotope fractionation factor. For a number of field studies, the Rayleigh equation has been used to evaluate whether field data follow a Rayleigh trend (*1*, *8*, *9*), to calculate the extent of contaminant biodegradation (*1*−*6*, *9*, *13*, *14*), or to estimate first-order rate constants by combining the Rayleigh equation with the first-order rate law (*14*). In the first case, the goal is usually to substantiate the importance of reactive processes and not to derive field-based isotope enrichment factors for further use. Field-based isotope enrichment factors can provide some indications on the relative importance of reactive versus nonreactive processes on the concentration decrease.

Although the Rayleigh equation was originally developed for homogeneous batch systems (*18*), it is increasingly applied for flow-through systems such as column and field studies (*1*−*9*, *11*−*15*). In a flow through system, physical and chemical heterogeneity influences the interpretation of isotope data and is expected to lead to an underestimation of the amount of biodegradation when the Rayleigh equation is applied, as recently shown by Kopinke et al. 2005 (*17*). Due to physical heterogeneity, the travel time of contaminants between the source and a monitoring point varies depending on the flow path. In addition, reaction rates can vary between and within different flow paths due to changes in geochemical conditions and microbial populations (hereafter referred to as chemical heterogeneity). Finally, the observed shift in isotope ratios in the bulk aqueous phase may not adequately reflect isotope fractionation at the microscale due to mass transfer limitations (*17*). The main aim of this study is to quantify the effect of physical heterogeneity on the estimation of isotope enrichment factors, the extent of biodegradation, or first-order rate constants using Rayleigh-type isotope data analysis. In addition, some calculations were carried out to evaluate the effect of chemical heterogeneity.

At field sites, groundwater flow velocity varies as a function of physical heterogeneity. As a result, groundwater samples contain a mixture of contaminant molecules that have traveled at a variety of velocities between the source and a sampling point. The contaminants were thus subject to a variety of residence times and, consequently, underwent various degrees of biodegradation. When the resultant average concentrations and isotope ratios are used to quantify isotope enrichment factors, the extent of biodegradation, and biodegradation rates, a systematic effect may be introduced because the Rayleigh equation relies on the assumption that the system is homogeneous. In this study, the following approach was chosen to quantify this effect: (1) Contaminant concentrations and isotope ratios were simulated, taking into account travel time variations between the source and an observation point. (2) The obtained data were evaluated to estimate isotope enrichment factors, the extent of biodegradation, and degradation rates using the Rayleigh equation. (3) The systematic effect was evaluated by comparing the obtained parameters with the "true" parameters used as input parameters in the calculations or with the true decrease in concentration derived from the calculations. An analytical approach was used to simulate concentrations and isotope ratios rather than a numerical approach because it allowed a rapid evaluation of a large number of field scenarios. The evaluated scenarios included

* Corresponding author phone: ++ 41 32 718 25 60; fax: ++ 41 32 718 26 03; e-mail: Daniel.Hunkeler@unine.ch.

various dispersive conditions, various degrees of biodegradation, as well as various plume geometries. The effect of chemical heterogeneity was evaluated by varying the degradation rate as a function of travel time, although this approach does not cover all possible effects of chemical heterogeneity. In addition to the systematic effect, the calculated entities are also affected by uncertainty in the analytical data and uncertainty in the parameters used to calculate them. For comparison, the uncertainty due to these factors was also quantified and is denoted as random uncertainty. Finally, the systematic effect and random uncertainty associated with the application of the Rayleigh equation was estimated for a number of published field studies.

Theory and Modeling

Simulation of Concentrations and Isotope Data. Concentrations and isotope ratios were simulated for field scenarios with various levels of physical heterogeneity using a Lagrangian approach. According to this approach, the travel time distribution is conceptualized by tagged fluid particles traveling at different velocities along separate flow paths (streamlines) of various tortuosity (*19*). Exchange of mass between streamlines and pore-scale dispersion are not considered. Thus, the spreading of a plume occurs mainly from differences in velocity at the macroscopic scale rather than at the microscopic scale (*20*). This representation of physical heterogeneity corresponds to the concept of segregated flow for nonideal reactors in chemical engineering (*17*, *21*). The Lagrangian approach has the advantage that transport and reaction can be treated separately (*19*, *22*). Solute transport between the source and a control plain located at a distance x can be characterized by a probability density function (PDF) $g(\tau, x)$ for the travel time τ of a conservative solute, while reactions are described by a reaction function. The reaction function $\Gamma(\tau, t)$ describes the progress of a reaction with respect to the travel time τ of a tagged particle and the time t, which corresponds to the elapsed time since emplacement of the source. The normalized breakthrough curve of a reacting compound is obtained by combining the travel time PDF with the reaction function according to eq 1.

$$c(t,x) = C(t,x)/C_0 = \int_\tau g(\tau,x)\Gamma(\tau,t)d\tau \qquad (1)$$

In this study, an analogous approach is used to characterize transport and degradation of a compound between the source area and a monitoring well. The monitoring well is considered to sample a number of streamlines representing different travel times. To reproduce breakthrough curves at monitoring wells, the travel time PDF and the reaction function need to be defined. The travel time PDF can be obtained in different ways: by simulating the response of an instantaneous tracer injection using analytical (*23*, *24*) or numerical models (*25*) or by deriving it from stochastic properties of the hydraulic conductivity (*26*). In this study, the travel time PDF was characterized by an analytical solution to the advection−dispersion equation. This approach has the advantage that deviations from the Rayleigh-type behavior can be rapidly assessed for a wide range of various parameters. The proposed method can also be incorporated with any other travel time PDF. The 2D solution was selected for the travel time PDF because field sites are frequently equipped with fully screened monitoring wells, which sample the average concentrations over a certain depth interval. Furthermore, tracer experiments are frequently carried out with such monitoring wells; thus, the derived dispersion coefficients represent travel time variations within a certain depth interval of the aquifer. Finally, transverse dispersion in the vertical direction is usually considered to be relatively insignificant in comparison to dispersion in other directions (*27*).

The travel time PDF is given as follows (*23*, *24*):

$$g(\tau,x,y) = \frac{x}{4\sqrt{\pi D_x \tau^3}} \cdot \exp\left[-\frac{(x-v\tau)^2}{4D_x\tau}\right] \cdot \left\{ erfc\left[\frac{y-w/2}{2\sqrt{D_y\tau}}\right] - erfc\left[\frac{y+w/2}{2\sqrt{D_y\tau}}\right]\right\} \qquad (2)$$

where x is the longitudinal distance of a monitoring point from the source, y is the lateral distance from the center of the plume, D_x is the longitudinal dispersion coefficient, v is the average groundwater flow velocity, w is the width of the source, and D_y is the transverse dispersion coefficient. This equation is obtained by the integration of the solution for a point injection with a Dirac pulse as initial condition along the y axes (*23*). Biodegradation of the organic compounds is described by first-order degradation kinetics, and the reaction function is given by eq 3:

$$\Gamma(\tau,t) = e^{-k\cdot\tau} H(t-\tau) \qquad (3)$$

where k is the first-order rate constant, and H is the Heaviside function. In the following sections, it is assumed that t is much larger than τ, the travel time between the source and a monitoring well. In other words, the plumes are considered to be stationary. Therefore, $H(t\text{-}\tau)$ corresponds to 1, and the concentration observed at x is independent of t. It is noteworthy to point out that the integral of eq 2 with respect to τ is smaller than 1 because of the transverse dispersion.

Substitution of eqs 2 and 3 into eq 1 and application of the dimensionless parameters given below yields the following expression:

$$\frac{C(X_D,Y_D)}{C_0} = c(X_D,Y_D) = \int_T \frac{\sqrt{PeX_D}}{4\sqrt{\pi T^3}} \exp\left[-\frac{Pe(X_D-T)^2}{4TX_D} - DaT\right] \times \left[erfc\left(\frac{Y_D-1}{2\sqrt{\frac{X_D T G^2}{FPe}}}\right) - erfc\left(\frac{Y_D+1}{2\sqrt{\frac{X_D T G^2}{FPe}}}\right)\right] dT \qquad (4)$$

with this:

$$c = \frac{C}{C_0} \qquad Pe = \frac{xv}{D_x} = \frac{x}{\alpha_x} \qquad T = \frac{v\tau}{x_R} = \frac{\tau}{\bar{\tau}}$$

$$X_D = \frac{x}{x_R} \qquad Y_D = \frac{y}{w/2} \qquad G = \frac{x_R}{w/2}$$

$$Da = \frac{kx_R}{v} = k\bar{\tau} \qquad F = \frac{\alpha_x}{\alpha_y}$$

Where c is the dimensionless concentration, C is the concentration, C_0 is the initial concentration, X_D is the dimensionless distance from the source, Y_D is the lateral dimensionless distance from the center of the plume, Pe is the Peclet number, α_x the longitudinal dispersivity, α_y is the transverse dispersivity, F is the ratio between longitudinal and transverse dispersivities often considered to be 10 (*27*, *28*), x_R is the distance of a sampling point from the source, $\bar{\tau}$ is the mean travel time between the source and the sampling point at x_R ($\bar{\tau} = x_R/v$), G is the location of the sampling point along the flow direction relative to the half source width, and Da is the Damköhler number. There are different definitions of the Damköhler number (*21*, *29*), and the one we chose

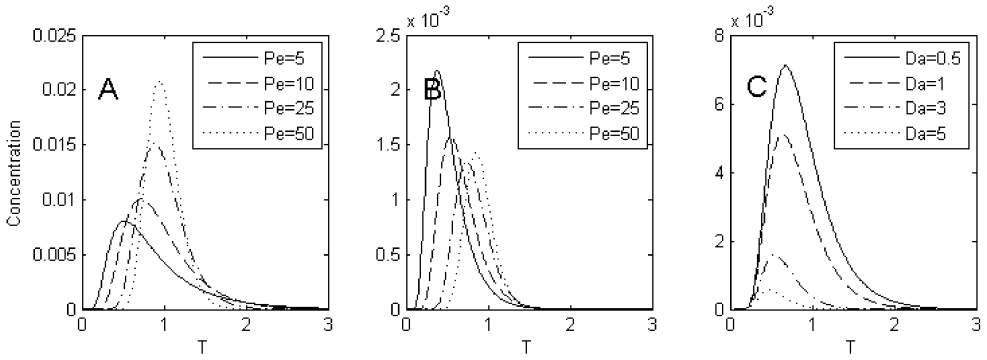

FIGURE 1. Simulated breakthrough curves: (A) without degradation; (B) with degradation at *Da* = 3; and (C) with various degree of degradation at *Pe* = 10.

relates the rate of advective transport to the rate of degradation. A large *Da* indicates that degradation is fast compared to transport and vice-versa. The Peclet number represents the dominance of advection over dispersion; thus, higher *Pe* suggests an advection-dominant flow condition and vice versa. According to the definition of *Pe* above, the dispersivity increases with travel distance, as often observed at field sites (*28*, *30*−*32*), by holding *Pe* constant. *G* can be roughly seen as the plume geometry with respect to the source width, and it varies considerably (*8*, *33*−*35*).

Equation 4 was numerically integrated with respect to *T*, although an approximate solution exists (*36*) and has been used widely in common analytical models such as BIOCHLOR (*37*) and BIOSCREEN (*38*). The approximate solution was used to estimate the velocity of groundwater (*39*), the contaminant plume length (*40*), and the first-order rate constant (*41*). However, this solution is prone to an increased level of errors, especially outside of the plume centerline in comparison to the numerically integrated solution (*42*). Therefore, numerical integration is used in this study. Numerical integration was carried out with Matlab using the adaptive Lobatto quadrature function. Using the integrand of eq 4, breakthrough curves (BTC) were generated to visualize the travel time distribution of molecules arriving at the sampling point (Figure 1). As the flow becomes dispersion dominated (smaller *Pe* values), the peak of the BTC shifts to earlier travel times. This trend is further enhanced as the degree of biodegradation increases (larger *Da* values).

Equation 4 was used to calculate the concentration decrease between the source and a monitoring point. To obtain the isotope ratio at the monitoring point, using carbon as an example, eq 4 was computed separately for ^{13}C and ^{12}C under identical conditions, except for the Damköhler number. The Damköhler numbers for ^{13}C and ^{12}C are related by the isotope fractionation factor, α, as follows:

$$\alpha = \frac{^{13}Da}{^{12}Da} \tag{5}$$

The expected isotope ratio at a given location divided by the initial isotope ratio is given by the following:

$$\frac{R(X_D,Y_D)}{R_0} = \frac{C_{13}(X_D,Y_D)/C_{13,0}}{C_{12}(X_D,Y_D)/C_{12,0}} = \frac{c_{13}(X_D,Y_D)}{c_{12}(X_D,Y_D)} \tag{6}$$

This approach can be considered to represent the behavior of organic compounds that are degraded throughout the contaminant plume and not only at the fringes of the plume.

Evaluation of Simulated Data and Quantification of Uncertainty. Equations 4 and 6 were used to simulate changes in concentrations and isotope ratios, respectively, between the source and a monitoring point for various scenarios. The resulting data were evaluated to derive isotope enrichment factors, the extent of biodegradation, and first-order degradation rate constants using the Rayleigh equation as described below. The obtained values were compared with the true values to estimate the systematic effect associated with the application of the Rayleigh equation. The deviation from the true values was evaluated as a function of variable dispersion, which reflects variable degrees of physical heterogeneity (*Pe*), different ratios between plume length and plume width (*G*), and different degrees of biodegradation (*Da*). The dimensionless parameters were varied as follows: (1) *Pe* was varied between 1 and 50, (2) *G* was varied between 1 and 20 based on typical values observed at field sites (see Table S1 in the Supporting Information), and (3) *Da* was varied between 1 and 10. For comparison, the random uncertainty due to uncertainties of the analytical method and the chosen isotope enrichment factor was also calculated for the extent of biodegradation *B* and first-order rate constant *k*.

Estimation of Isotope Enrichment Factors. Although it is generally accepted that isotope enrichment factors should be determined by laboratory experiments, it can be of interest to estimate field-based isotope enrichment factors and to compare them with laboratory-based values. Such a comparison can provide some insight into the overall contribution of biodegradation to the observed concentration decrease. Therefore, we evaluate the relationship between field-estimated and laboratory-derived isotope enrichment factors. To simulate the estimation of isotope enrichment factors from field data, concentrations and isotope ratios were calculated using eqs 4 and 6 for a set of 10 dimensionless distances, X_D, between 0.1 and 1 at intervals of 0.1. Unless otherwise specified, *Da* was set to 3, corresponding to 95% biodegradation between the source and the most downgradient sampling point (x_R). Based on the 10 data points, the isotope enrichment factor was estimated using the Rayleigh equation and least-squares linear regression:

$$1000\ln\left(\frac{R}{R_0}\right) = \epsilon_{\text{Rayleigh}}\ln[f] \tag{7}$$

where $f = C/C_0$. Here f is given by $c(X_D, Y_D)$, calculated from eq 4. The obtained isotope enrichment factor $\epsilon_{\text{Rayleigh}}$ was compared to the true isotope enrichment factor ϵ_{true} ($\epsilon_{\text{true}} = (\alpha - 1)1000$) where α is the original isotope fractionation factor used in eq 5 for the simulation of isotope ratios.

Estimation of the Fraction Remaining or Extent of Biodegradation. The fraction remaining, *f*, is given by eq 8.

$$f_{\text{Rayleigh}} = \left(\frac{R}{R_0}\right)^{1000/\epsilon_{\text{true}}} \tag{8}$$

Instead of the fraction remaining, the result is often presented as a fraction biodegraded in percentages (*6*):

$$B_{\text{Rayleigh}}\,(\%) = (1 - f_{\text{Rayleigh}})100 \quad (9)$$

In this study, f and B were calculated based on eqs 8 and 9, with the ratio R/R_0 obtained from eq 6, and they are denoted as f_{Rayleigh} and B_{Rayleigh}, respectively. According to the Rayleigh equation (eq 7), f_{Rayleigh} should correspond to C/C_0. However, the concentration also decreases due to hydrodynamic dispersion; therefore, f_{Rayleigh} was compared to the fraction remaining relative to the contaminant concentration that would be expected if no degradation occurs (for comparison, see Figure S1 in the Supporting Information):

$$f_{\text{true}} = \frac{C}{C_{\text{dispersion}}} \quad (10)$$

where C is the concentration remaining due to the effect of dispersion and degradation, and $C_{\text{dispersion}}$ is the concentration remaining in the absence of biodegradation. In this study, f_{true} was calculated by dividing eq 4 by an analogous equation with $Da = 0$ to simulate a nondegrading conservative tracer, and B_{true} was obtained by $B_{\text{true}} = (1 - f_{\text{true}})100$. Again, the calculated f_{Rayleigh} and B_{Rayleigh} values are compared to their reference values, f_{true} and B_{true}, to characterize the systematic effect.

The random uncertainty of B due to the uncertainties associated with R, R_0, and ϵ was evaluated based on eqs 8 and 9 whereby R and R_0 were assumed to have the same uncertainty linked to the analytical method. Differentiating eq 9 with respect to ϵ and R, and applying the law of the propagation of uncertainty, the following expressions are obtained for the random uncertainty of B estimations:

$$\left(\frac{\partial B_{\text{Rayleigh}}}{B_{\text{Rayleigh}}}\right)^2 = \left(\frac{\exp(-Da)}{1-\exp(-Da)}\right)^2\left[Da^2\left(\frac{\partial \epsilon_{\text{true}}}{\epsilon_{\text{true}}}\right)^2 + 2\left(\frac{1000}{\epsilon_{\text{true}}}\right)^2\left(\frac{\partial R}{R}\right)^2\right] \quad (11)$$

where ∂f, ∂R, and $\partial \epsilon$ are the standard deviations of the corresponding parameters. For this study, the relative uncertainty of R ($\partial R/R$), caused by measurement uncertainty, was assumed to correspond to the typical analytical uncertainty of 0.03%. The $\partial \epsilon/\epsilon$ were assumed to vary between 10 and 50%, corresponding to the typical range of the standard deviations for a compound if all published values for isotope enrichment factors are taken into account.

Estimation of First-Order Rate Constants. First-order rate constants can be estimated from calculated isotope ratios by combining the Rayleigh equation with the first-order rate law to substitute f as $f = \exp(-k\bar{\tau})$ (*14*, *15*):

$$\ln\left(\frac{R}{R_0}\right) = -\frac{\epsilon_{\text{true}}}{1000}k_{\text{Rayleigh}}\cdot\bar{\tau} \quad (12)$$

Accordingly, the estimated rate constant is given by eq 13.

$$k_{\text{Rayleigh}} = -\frac{\frac{1000}{\epsilon_{\text{true}}}\cdot\ln\left(\frac{R}{R_0}\right)}{\bar{\tau}} = -\frac{\ln(f_{\text{Rayleigh}})}{\bar{\tau}} \quad (13)$$

The true rate constant can be obtained by manipulating the definition of the Damköhler number since it is a function of k:

$$k_{\text{true}} = \frac{Da}{\bar{\tau}} \quad (14)$$

The systematic effect, the ratio between estimated and true rate constant, therefore, corresponds to the following:

$$\frac{k_{\text{Rayleigh}}}{k_{\text{true}}} = \frac{\frac{1000}{\epsilon_{\text{true}}}\ln\left(\frac{R}{R_0}\right)}{Da} = -\frac{\ln(f_{\text{Rayleigh}})}{\bar{\tau}} \quad (15)$$

where R/R_0 was calculated using eq 6.

As in the estimation of random uncertainties of f and B, the random uncertainty of k due to the uncertainties of ϵ, $\bar{\tau}$, and R is derived from differentiating eq 13 and is given by eq 16. Similarly as for B, the relative uncertainty of R ($\partial R/R$)

$$\left(\frac{\partial k_{\text{Rayleigh}}}{k_{\text{Rayleigh}}}\right)^2 = \left(\frac{\partial \epsilon_{\text{true}}}{\epsilon_{\text{true}}}\right)^2 + \left(\frac{\partial \bar{\tau}}{\bar{\tau}}\right)^2 + 2\left(\frac{1000}{Da\epsilon_{\text{true}}}\right)^2\left(\frac{\partial R}{R}\right)^2 \quad (16)$$

was assumed to correspond to 0.03%, and $\partial \epsilon/\epsilon$ was varied between 10 and 50%. In addition, $\partial \bar{\tau}/\bar{\tau}$ was assumed to correspond to 20%.

Results and Discussion

Estimation of Isotope Enrichment Factors. In Figure 2, the relationship between the isotope enrichment factor derived from the simulated data set ($\epsilon_{\text{Rayleigh}}$) and the isotope enrichment factor used to generate the data set (ϵ_{true}) is illustrated in the form of type curves for various *Pe*, *Da,* and *G*. The estimated $\epsilon_{\text{Rayleigh}}$ always underestimates ϵ_{true}. As *Pe* becomes larger, or the flow becomes advection-dominant, the effect becomes smaller due to a narrower travel time PDF (Figure 1A). Therefore, when *Pe* is large, as in the column studies, the systematic effect is minimized, whereas when *Pe* is smaller, as in field studies, the effect varies significantly with the chosen dimensionless parameters. Figure 2A demonstrates that for large *Da* values, corresponding to the relatively fast degradation compared to migration, greater deviation from ϵ_{true} values is expected. For a large *Da*, the measured isotope ratio is dominated by molecules with a short residence time (Figure 1C) corresponding to a relatively small shift in δ^{13}C. Accordingly, the calculated $\epsilon_{\text{Rayleigh}}$ is smaller than ϵ_{true}. The $\epsilon_{\text{Rayleigh}}/\epsilon_{\text{true}}$ ratio is also sensitive to *G* (Figure 2B). Larger *G* corresponds to a longer plume relative to the source width. The longer the plume, the more the concentrations are diminished due to transverse dispersion in addition to biodegradation; therefore, the underestimation of ϵ is enhanced with increasing *G*. For a typical *Pe* of 10 and typical ratios of plumes lengths to source widths of up to 20, $\epsilon_{\text{Rayleigh}}$ is expected to be as much as 50% smaller than ϵ_{true}. The magnitude of the systematic effect associated with the ϵ calculation was estimated for a published MTBE field study (*9*, *43*). Because the study reported laboratory ϵ value derived from microcosms with site material, the model-predicted underestimation of ϵ can be compared to the actual underestimation of ϵ. To calculate the systematic effect, dimensionless parameters, *Pe*, *G,* and *Da*, were estimated based on site specific data. *Pe* was assumed to correspond to a typical value of 10. *G* was estimated based on the location of the most downgradient well for two source widths of 10 and 20 m because the actual source width was unknown. *Da* was estimated to be 2.4 based on the δ^{13}C of the most downgradient well and the corresponding isotope enrich-ment factor from the laboratory study. The ratio $\epsilon_{\text{Rayleigh}}/\epsilon_{\text{true}}$ was calculated as described in the method section except that X_D values were selected according to the locations of the sampling wells. According to these calculations, the ratio $_{\text{Rayleigh}}/\epsilon_{\text{true}}$ amounts to 0.55−0.59 (Table 1). This corresponds well to the ratio between field- and laboratory-based isotope enrichment factors, $\epsilon_{\text{field}}/\epsilon_{\text{lab}}$, which was 0.62. The good agreement between estimated and actually observed ratios suggests that the factors incorporated into our approach

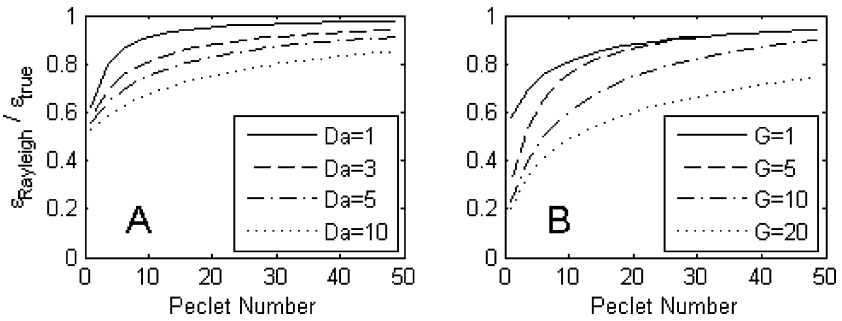

FIGURE 2. Type curves for the systematic effect (expressed as $\epsilon_{Rayleigh}/\epsilon_{true}$) associated with estimating isotope enrichment factors: (A) assuming $G = 1$ with 4 different Da values and (B) assuming $Da = 3$ with 4 different G values.

TABLE 1. Systematic Effect of Isotope Enrichment Factor Derived from Field Data Expressed as $\epsilon_{Rayleigh}/\epsilon_{True}$ and Comparison with $\epsilon_{Field}/\epsilon_{Lab}$

	MTBE
ϵ_{field} [‰]	−8.1
ϵ_{lab} [‰] (reference)	−13 ± 1.1[a] (43)
$\epsilon_{field}/\epsilon_{lab}$	0.62
$\epsilon_{Rayleigh}/\epsilon_{true}$	0.55 (w=10m)
	0.59 (w=20m)

[a] 95% confidence interval as given in ref 43.

(travel time distribution due to hydrodynamic dispersion) are responsible for the underestimation of ϵ based on field isotope data.

Estimation of the Extent of Biodegradation. The expected systematic effect associated with assessing the extent of biodegradation, B, from field isotope data is illustrated in Figure 3. As in the estimation of ϵ, isotope data led to the underestimation of the actual B, particularly under dispersion-dominant flow conditions (low Pe region). The systematic effect for estimating B is smaller than for estimating ϵ and independent of G (Figure 3B). These observations can be explained by the fact that dilution due to transverse dispersion hardly affects isotope ratios, but strongly affects concentrations.

For groundwater risk assessment, the fraction of contamination remaining after a certain distance is often of key interest, which corresponds to f (*44*). The calculated $f_{Rayleigh}$ can be up to 5 times larger than the actual f_{true} for $Pe = 10$ and G up to 20 (see Figure S2 in the Supporting Information). However, a systematic effect of f by a factor of up to 5 remains quite small compared to the concentration decrease, which is often several orders of magnitude. The different behavior of the systematic effect of f, compared to B, is expected because f approaches 0 as the degree of degradation increases, while B approaches 1. As a result, the systematic effect on f increases with increasing Da, while the systematic effect on B becomes small.

The degree of random uncertainty associated with estimating B is plotted in Figure 4 as a function of Da for two different isotope enrichment factors. Similar to the systematic effect discussed above, the random uncertainty of B decreases as a function of Da, as previously observed (*45*). For $Da <$ 5, the uncertainty of B is slightly smaller for the smaller isotope enrichment factor and increases with increasing uncertainty of ϵ. For small Da, corresponding to small shifts in isotope ratios, the random uncertainty is dominated by the uncertainty on the isotope analysis ($\partial R/R$), while for larger Da, the contribution of the uncertainty associated with the isotope enrichment factor is dominant (Figure 4C).

For several published field sites, $B_{Rayleigh}$ values as well as the expected systematic effect and random uncertainty associated with them were calculated (*1*, *6*, *9*). The first example is the MTBE site, which was mentioned in the previous section, the second example is a BTEX/PAH contaminated site (*1*, *46*−*48*), and the third is a landfill site where mixed contamination was observed (*6*, *49*). The estimation of $B_{Rayleigh}/B_{true}$ ratio was performed for the monitoring well furthest from the source area based on the dimensionless parameters Pe, Da, and G (Table 2). The random uncertainty of $B_{Rayleigh}$ was quantified as described in the Theory and Modeling section (eq 11) using the parameters given in Table 2. It was assumed that $\partial R/R$ corresponds to 0.03%, and the uncertainty of ϵ was estimated for each compound separately based on laboratory ϵ values (Table 2). *m*/*p*-Xylene was not included because of the lack of sufficient ϵ values to calculate the standard deviation ($\partial\epsilon$). Calculated $B_{Rayleigh}/B_{true}$ ratios and $\partial B_{Rayleigh}/B_{Rayleigh}$ ratios are listed in Table 2.

The calculated $B_{Rayleigh}/B_{true}$ ratios indicate that the extent of biodegradation was underestimated by 2−10% for the considered sites and compounds (Table 2). The smallest systematic effect was observed for *o*-xylene, which showed the highest level of biodegradation. The random uncertainty ($\partial B/B$) was in the same range as the systematic effect except for benzene, which had a relative random uncertainty of 35%. The smallest random uncertainties (MTBE and *o*-xylene) occurred when either the uncertainty of the isotope enrich-

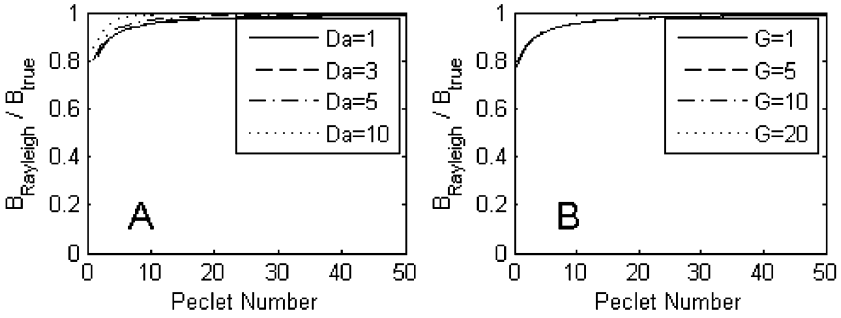

FIGURE 3. Type curves for the systematic effect (expressed as $B_{Rayleigh}/B_{true}$) associated with estimating the extent of biodegradation: (A) assuming $G = 1$ with 4 different Da values and (B) assuming $Da = 3$ with 4 different G values.

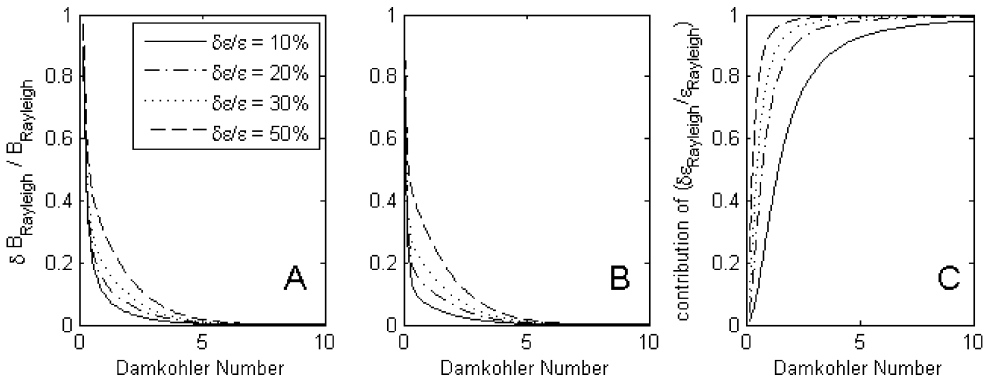

FIGURE 4. Random uncertainty of extent of biodegradation ($\partial B/B$) for (A) $\epsilon_{true} = 3‰$ and (B) $\epsilon_{true} = 10‰$ and (C) contribution of the uncertainty of ϵ ($\partial\ \epsilon_{true}/\epsilon_{true}$) to the overall random uncertainty. $\partial R/R$ held constant at 0.03%.

TABLE 2. Estimations of the Systematic Effect and Random Uncertainty Associated with the Rayleigh-Type Evaluation of Field Isotope Data

	MTBE site[b] (9)	BTEX/PAH site (1)				landfill site (6)
	MTBE	**benzene**	**toluene**	***o*-xylene**	***m/p*-xylene**	***m/p*-xylene**
v [m/d]	0.26	2	2	2	2	0.5
w [m]	10 & 20	120	120	120	120	270
x_R [m]	23.5	105	105	105	105	47
G	4.7 & 2.4	1.8	1.8	1.8	1.8	0.35
Pe at x_R	10	8.3[c]	8.3[c]	8.3[c]	8.3[c]	10
$\partial\epsilon/\epsilon$[d]	0.085	0.29	0.41	0.62		
(reference)	(43)	(50)	(51,52)	(5,45)		
Da at x_R	2.40	0.50	2.34	5.31	2.18	3.12
$B_{Rayleigh}$ [%]	91.1	39.5	90.4	99.5	88.7	95.6
$\mathbf{B_{Rayleigh}/B_{true}}$	**0.9**	**0.97**	**0.94**	**0.98**	**0.94**	**0.95**
$\mathbf{\partial B_{Rayleigh}/B_{Rayleigh}}$	**0.02**	**0.35**	**0.11**	**0.02**		
$\mathbf{k_{Rayleigh}\ [d^{-1}]}$	**0.0027**	**0.0099**	**0.046**	**0.104**	**0.029**	**0.023**
$k_{Rayleigh}/k_{true}$	0.71	0.88	0.68	0.53	0.70	0.67
$\mathbf{\partial k_{Rayleigh}/k_{Rayleigh}}$	**0.22**	**0.50**	**0.47**	**0.66**		

[a] Values in bold are the simulation results. [b] The calculation was carried out for two source widths. However, only one average result is reported because the calculation is not sensitive to the source width (Figure 3B and 5B). [c] Calculated based on results of tracer tests reported in ref *48*. For other sites a typical Pe of 10 was used. [d] Standard deviation calculated based on all values given in quoted references.

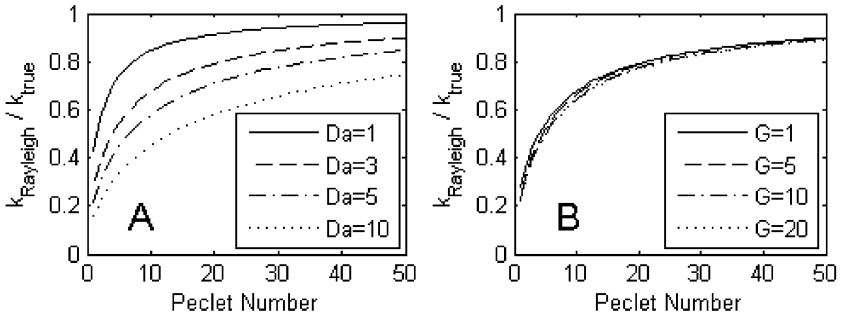

FIGURE 5. Type curves for the systematic effect (expressed as $k_{Rayleigh}/k_{true}$) associated with estimating the first-order reaction rate constant: (A) assuming $G = 1$ with 4 different *Da* values and (B) assuming $Da = 3$ with four different *G* values.

ment factor, $\partial\epsilon/\epsilon$, was very small (MTBE) or *Da* was large (*o*-xylene), resulting in a very small fraction of contaminant remaining. The large random uncertainty of benzene was due to the small *Da* and the relatively large uncertainty of ϵ. In summary, the calculations for the field sites and the general evaluations (Figures 3 and 4) indicate that, for $Da < 3$, the random uncertainty may frequently be more important than the systematic effect for a typical *Pe* of 10, unless the uncertainty of ϵ is very small. For larger *Da*, both the systematic effect and random uncertainty are expected to be small.

Estimation of First-Order Reaction Rate Constants. The systematic effect associated with the calculation of field-derived first-order rate constants is illustrated in Figure 5. The systematic effect on $k_{Rayleigh}$ depends significantly on *Da*, and is rather independent of *G* as in the case for the $B_{Rayleigh}$ estimation. As *Pe* increases, the effect decreases, but at the typical flow condition of $Pe = 10$, a significant systematic effect is involved (Figure 5A). The systematic effect on $k_{Rayleigh}$ is much larger than that on $B_{Rayleigh}$ and increases with increasing *Da*. The different behaviors in terms of expected systematic effect on $B_{Rayleigh}$ and $k_{Rayleigh}$ estimations arise from the fact that the $k_{Rayleigh}$ calculation is based on $f_{Rayleigh}$ (see eq 13). As discussed above, the systematic effect on $f_{Rayleigh}$ is larger than on $B_{Rayleigh}$ and increases with *Da*. For larger *Da*, molecules with a short residence time and, hence, little degradation are increasingly over-represented in the sample.

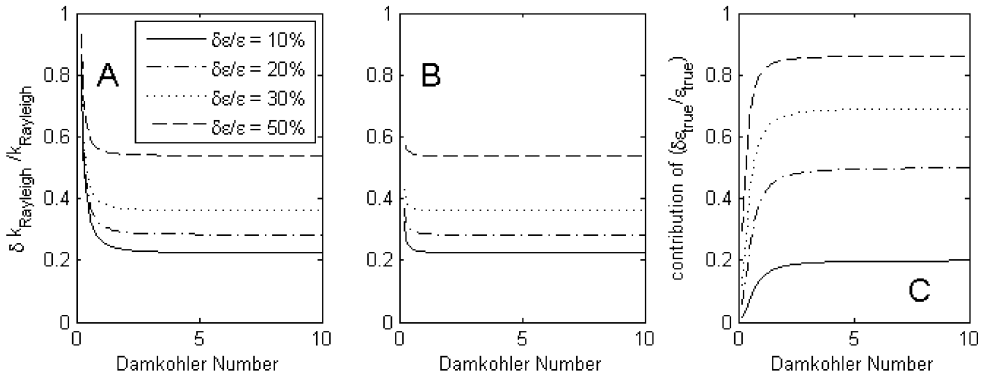

FIGURE 6. Random uncertainty of the estimation of first-order rate constants ($\partial k/k$) for (A) $\epsilon_{true} = 3‰$ and (B) $\epsilon_{true} = 10‰$ and (C) contribution of the uncertainty of ϵ_{true} ($\partial\ \epsilon_{true}/\epsilon_{true}$) to the overall random uncertainty. $\partial R/R$ held constant at 0.03%, and $\delta\bar{\tau}/\bar{\tau}$ at 20%.

The random uncertainty associated with estimating $k_{Rayleigh}$ is depicted in Figure 6 in terms of a series of $\partial\epsilon\ /\epsilon$ values for two different ϵ values as well as the expected contribution of $\partial\epsilon\ /\epsilon$ to the random uncertainty, $\partial k\ /k$. For a small *Da*, the systematic effect is large and is dominated by $\partial R\ /R$. For a larger *Da*, $\partial k\ /k$ stabilizes to a certain value depending on $\partial\epsilon\ /\epsilon$ and $\partial\bar{\tau}/\bar{\tau}$ (eq 16).

For the previously mentioned field studies (*1*, *6*, *9*), the systematic effect and random uncertainty of $k_{Rayleigh}$ were quantified for the most downgradient wells (Table 2). In addition, the $k_{Rayleigh}$ values were calculated using eq 13 where R and R_0 were calculated from the measured isotope ratios. The systematic effect was estimated using eq 15, and the random uncertainty was estimated using eq 16. The random uncertainty depends on $\delta\bar{\tau}/\bar{\tau}$ as much as it does on $\delta\epsilon\ /\epsilon$, but $\delta\bar{\tau}/\bar{\tau}$ is difficult to estimate. In the calculation, an uncertainty of 20% was assumed for $\delta\bar{\tau}/\bar{\tau}$.

The $k_{Rayleigh}/k_{true}$ ratio suggests an underestimation of $k_{Rayleigh}$ of up to 47%. The random uncertainty on the $k_{Rayleigh}$ estimation is rather large, particularly for the BTEX/PAH site and reaches up to 66%. In contrast to $B_{Rayleigh}$, the random uncertainty is the largest for the compound with the largest *Da*. For larger uncertainty in average travel time ($\bar{\tau}$), the uncertainty will be even larger.

Effect of Chemical Heterogeneity. In addition to the effect of physical heterogeneity, the Rayleigh-type data interpretation is expected to be affected by variations of degradation rates between and along flow paths that are sampled. While there are a number of detailed studies about spatial variations of redox conditions within a plume (*33*, *39*, *53*, *54*), less is known about the spatial variation of degradation rates of organic compounds. Some studies have indicated that degradation rates are lower in low permeability zones (*33*, *55*). In this case, degradation rates would be related to travel time with faster flow paths showing higher rates. To simulate the effect of such a relationship on the systematic effect of *B*, the Damköhler number was linearly varied as a function of travel time with decreasing *Da* for increasing *T*. The total amount of biodegradation between the source and a sampling point was kept constant and corresponded to $Da = 3$ (see Figure S3 in the Supporting Information). The slope *s* of the *Da* vs *I* relationship varied between −0.3 and −1.2. The different scenarios correspond to a decrease of 10, 20, and 40%, respectively of the degradation rate if the travel time is doubled from one *T* to two *T*. The systematic effect decreases with increasing slope *s* (Table 3). As discussed above, the systematic effect for *B* is due to the fact that molecules with a short travel time, thus a small shift in $\delta^{13}C$, are overrepresented in the sample. If the degradation rate is higher for faster flow paths, this overrepresentation is diminished, consequently the systematic effect is smaller. If the relationship between degradation rate and travel time is inverse, the systematic effect increases (data not shown). In this case, the sample is dominated by molecules from fast flow paths with hardly any degradation and hardly any shift in $\delta^{13}C$. If the representative parameters for chemical heterogeneity, such as a degradation rate, are not correlated with travel time, the error could lead to an increase or a decrease depending on the scenario considered, and the exact effect from such chemical heterogeneity is difficult to quantify.

TABLE 3. Effect of Simulated Chemical Heterogeneity on $B_{Rayleigh}/B_{True}$.[a]

s	$B_{Rayleigh}/B_{true}$
0	0.954
−0.3	0.954
−0.6	0.958
−1.2	0.979

[a] S corresponds to the rate at which Da decreases with increasing dimensionless travel time T.

Implication for the Application of the Rayleigh Equation at Field Sites. Presented type curves (Figures 2, 3, and 5) for systematic effects represent a large range of possible field scenarios; thus, they can serve as a reference to quickly estimate the degree of systematic effect associated with a site of interest. As expected, the Rayleigh-based approach to estimate the extent of biodegradation or first-order rate constants leads to a systematic underestimation of the actual value due to the fact that it does not accommodate the subsurface physical heterogeneity. Hence, it can be considered to provide a conservative estimate of these entities. As the degree of physical heterogeneity decreases (represented by advection, dominant flow regime, or high Peclet numbers), the systematic effect decreases significantly. For a typical *Pe* of 10, typical values for plume lengths ($G < 20$), and degree of degradation ($Da < 10$), the systematic effect on the extent of biodegradation is <5%. This indicates that the isotope method for quantification of biodegradation is quite robust. This conclusion is consistent with several field studies that indicated that the predicted degree of biodegradation corresponds well to the concentration decrease (*1*, *6*). A larger systematic effect is expected for first-order rate constants (up to 50%). However, other methods for estimation of field degradation rates that are based on concentration data likely yield much larger errors. For example Stenback et al. (2004) (*41*) demonstrated that rates calculated based on concentration data can vary by a factor of 3, depending on the chosen dispersion coefficients. The estimated systematic effect may be larger for certain scenarios of chemical heterogeneity (e.g., increasing degradation rates for increasing residence time). In addition, it has to be kept in mind that the evaluation relies on Fickian dispersion which may

not be exactly met at field sites. Often, the tailing of breakthrough curves is more pronounced than expected based on Fickian dispersion (*20*, *28*, *30*, *56*, *57*), accordingly the systematic effect would be somewhat larger than expected. However, the proposed method to estimate systematic effect associated with the application of the Rayleigh equation to heterogeneous field sites can be applied for any kind of travel time PDF as long as the corresponding breakthrough curves are given.

Acknowledgments

The project was supported by the Swiss National Science Foundation.

Supporting Information Available

Data justifying the range of values that were considered for *G*. It also provides information on the systematic effect on the fraction remaining *f* and a diagram illustrating the effect of chemical heterogeneity.

List of Symbols

α	Isotope fractionation factor
α_x [L]	Longitudinal dispersivity
α_y [L]	Transverse dispersivity
B [%]	Fraction of biodegradation
B_{true} [%]	True fraction of biodegradation
$B_{Rayleigh}$ [%]	Fraction of biodegradation estimated based on isotope data using laboratory derived "true" isotope enrichment factor
C [M/L^3]	Concentration
C_0 [M/L^3]	Initial concentration
c	Dimensionless concentration
Da	Damköhler number
D_x [L^2/T]	Longitudinal dispersion coefficient
D_y [L^2/T]	Transverse dispersion coefficient
ϵ [‰]	Isotope enrichment factor
ϵ_{true} [‰]	True isotope enrichment factor derived from laboratory experiment
$\epsilon_{Rayleigh}$ [‰]	Isotope enrichment factor estimated from field data
f	Fraction remaining
F	Ratio of longitudinal to transverse dispersivities
g	Travel time PDF
Γ	Reaction function
G	Distance of sampling point relative to source half-width
k [T^{-1}]	First-order rate constant
k_{true} [T^{-1}]	True first-order rate constant (used to simulate data)
$k_{Rayleigh}$ [T^{-1}]	First-order rate constant estimated based on isotope data using laboratory derived "true" isotope enrichment factor
Pe	Peclet number
R	Isotope ratio
R_0	Initial isotope ratio
t [T]	Elapsed time since the source emplacement
τ [T]	Travel time
$\bar{\tau}$ [T]	Mean travel time
T	Dimensionless travel time
v [L/T]	groundwater flow velocity
w [L]	Width of the source
x [L]	Distance from source in flow direction
X_D	Dimensionless distance from source
x_R [L]	Distance of sampling point from source
y [L]	Lateral distance from center of plume
Y_D	Dimensionless lateral distance

Literature Cited

(1) Griebler, C.; Safinowski, M.; Vieth, A.; Richnow, H. H.; Meckenstock, R. U. Combined application of stable carbon isotope analysis and specific metabolites determination for assesing in site degradation of aromatic hydrocarbons in a tar oil-contaminated aquifer. *Environ. Sci. Technol.* **2004**, *38*, 617−631.

(2) Mancini, S. A.; Lacrampe-Couloume, G.; Jonker, H.; van Breukelen, B. M.; Groen, J.; Volkering, F.; Sherwood Lollar, B. Hydrogen isotopic enrichment: An indicator of biodegradation at a petroleum hydrocarbon contaminated field site. *Environ. Sci. Technol.* **2002**, *36*, 2464−2470.

(3) Meckenstock, R. U.; Morasch, B.; Kastner, M.; Vieth, A.; Richnow, H. H. Assessment of bacterial degradation of aromatic hydrocarbons in the environment by analysis of stable carbon isotope fractionation. *Water, Air, Soil Pollut.* **2002**, *2*, 141−152.

(4) Peter, A.; Steinbach, A.; Liedl, R.; Ptak, T.; Michaelis, W.; Teutsch, G. Assessing microbial degradation of *o*-xylene at field-scale from the reduction in mass flow rate combined with compound-specific isotope analyses. *J. Contam. Hydrol.* **2004**, *71*, 127−154.

(5) Richnow, H. H.; Annweiler, E.; Michaelis, W.; Meckenstock, R. U. Microbial in situ degradation of aromatic hydrocarbons in a contaminated aquifer monitored by carbon isotope fractionation. *J. Contam. Hydrol.* **2003**, *65*, 101−120.

(6) Richnow, H. H.; Meckenstock, R. U.; Reitzel, L. A.; Baun, A.; Ledin, A.; Christensen, T. H. In situ biodegradation determined by carbon isotope fractionation of aromatic hydrocarbons in an anaerobic landfill leachate plume (Vejen, Denmark). *J. Contam. Hydrol.* **2003**, *64*, 59−72.

(7) Stehmeier, L. G.; Francis, M. M.; Jack, T. R.; Diegor, E.; Winsor, L.; Abrajano, T. A., Jr. Field and in vitro evidence for in-situ bioremediation using compound-specific $^{13}C/^{12}C$ ratio monitoring. *Org. Geochem.* **1999**, *30*, 821−833.

(8) Steinbach, A.; Seifert, R.; Annweiler, E.; Michaelis, W. Hydrogen and carbon isotope fractionation during anaerobic biodegradation of aromatic hydrocarbons-A field study. *Environ. Sci. Technol.* **200**4, *38*, 609−616.

(9) Kolhatkar, R.; Kuder, T.; Philip, P.; Allen, J.; Wilson, J. T. Use of compound-specific stable carbon isotope analyses to demonstrate anaerobic biodegradation of MTBE in groundwater at a gasoline release site. *Environ. Sci. Technol.* **2002**, *36*, 5139−5146.

(10) Zwank, L.; Berg, M.; Elsner, M.; Schmidt, T. C.; Schwarzenbach, R. P.; Haderlein, S. B. New evaluation scheme for two-dimensional isotope analysis to decipher biodegradation processes: Application to groundwater contamination by MTBE. *Environ. Sci. Technol.* **2005**, *39*, 1018−1029.

(11) Sturchio, N. C.; Clausen, J. L.; Heraty, L. J.; Huang, L.; Holt, B. D.; Abrajano, T. A., Jr. Chlorine isotope investigation of natural attenuation of trichloroethene in an aerobic aquifer. *Environ. Sci. Technol.* **1998**, *32*, 3037−3042.

(12) Song, D. L.; Conrad, M. E.; Sorenson, K. S.; Alverez-Cohen, L. Stable carbon isotope fractionation during enhanced in situ bioremediation of trichloroethene. *Environ. Sci. Technol.* **2002**, *36*, 2262−2268.

(13) Sherwood Lollar, B.; Slater, G. F.; Sleep, B.; Witt, M.; Klecka, G. M.; Harkness, M.; Spivack, J. Stable carbon isotope evidence for intrinsic bioremediation of tetrachloroethene and trichlorothene at Area 6, Dover Air Force Base. *Environ. Sci. Technol.* **2001**, *35*, 261−269.

(14) Morrill, P. L.; Lacrampe-Couloume, G.; Slater, G. F.; Sleep, B.; Edwards, E. A.; McMaster, M. L.; Major, D. W.; Sherwood Lollar, B. Quantifying chlorinated ethene degradation during reductive dechlorination at Kelly AFB using stable carbon isotopes. *J. Contam. Hydrol.* **2005**, *76*, 279−293.

(15) Hunkeler, D.; Aravena, R.; Butler, B. J. Monitoring microbial dechlorination of tetrachloroethene (PCE) in groundwater using compound-specific stable carbon isotope ratios: Microcosm and field studies. *Environ. Sci. Technol.* **1999**, *33*, 2733−2738.

(16) Meckenstock, R. U.; Morasch, B.; Griebler, C.; Richnow, H. H. Stable isotope fractionation analysis as a tool to monitor biodegradation in contaminated aquifers. *J. Contam. Hydrol.* **2004**, *75*.

(17) Kopinke, F. D.; Georgi, A.; Voskamp, M.; Richnow, H. H. Carbon isotope fractionation of organic contaminants due to retardation on humic substances: Implications for natural attenuation studies in aquifers. *Environ. Sci. Technol.* **2005**, *39*, 6052−6062.

(18) Clark, I. D.; Fritz, P. *Environmental Isotopes in Hydrogeology*; Lewis Publishers: Boca Raton, Florida, USA, 1997.

(19) Cvetkovic, V.; Dagan, G. Transport of kinetically sorbing solute by steady random velocity in heterogeneous porous formations. *J. Fluid Mech.* **1994**, *265*, 189−215.

(20) Dagan, G. Time-dependent macrodispersion for solute transport in anisotropic heterogeneous aquifers. *Water Resour. Res.* **1988**, *24*, 2031−2046.

(21) Weber, W. J. J.; DiGiano, F. A. *Process Dynamics in Environmental Systems*; John Wiley & Sons: N. Y., 1996.

(22) Finkel, M.; Liedl, R.; Teutsch, G. Modelling surfactant influenced PAH migration. *Phys. Chem. Earth* **1998**, *23*, 245−250.

(23) Lenda, A.; Zuber, A. In *Symposium on the use of isotopes in Hydrology*; I. A. E. A.: Vienna, 1970; pp 619−641.

(24) Wexler, E. J. "Analytical solutions for one-, two-, and three-dimensional solute transport in groundwater systems with uniform flow," Techniques of Water Resources Investigations of the United States Geological Survey; U.S. Government Printing Office, Washington, DC, 1992.

(25) Cornaton, F. *Deterministic Models of Groundwater Age, Life Expectancy & Transit Time Distributions in Advective-Dispersive Systems. Ph.D. Thesis*, University of Neuchatel, Switzerland, 2004.

(26) Dagan, G. *Flow and Transport in Porous Formations*; Springer-Verlag: New York, 1989.

(27) Charbeneau, R. J. *Groundwater Hydraulics and Pollutant Transport*; Prentice-Hall: Upper Saddle River, NJ, 2000.

(28) Gelhar, L. W.; Welty, C.; Rehfeldt, K. R. A critical review of data on field-scale dispersion in aquifers. *Water Resour. Res.* **1992**, *28*, 1955−1974.

(29) Schwarzenbach, R.; Gschwend, P.; Imboden, D. *Environmental Organic Chemistry*, 2 ed.; John Wiley & Sons: New York, USA, 2003.

(30) Hess, K. M.; Wolf, S. H.; Celia, M. A. Large-scale natural gradient tracer test in sand and gravel, Cape Cod, Massachusetts 3. Hydraulic conductivity variability and calculated macrodispersivities. *Water Resour. Res.* **1992**, *28*, 2011−2027.

(31) Domenico, P. A.; Robbins, G. A. A dispersion scale effect in model calibration and field tracer experiments. *J. Hydrol.* **1984**, *70*, 123−132.

(32) Rajaram, H.; Gelhar, L. W. Plume-scale dependent dispersion in aquifers with a wide range of scales of heterogeneity. *Water Resour. Res.* **1995**, *31*, 2469−2482.

(33) Cozzarelli, I. M.; Bekins, B. A.; Baedecker, M. J.; Aiken, G. R.; Eganhouse, R. P.; Tuccillo, M. E. Progression of natural attenuation processes at a crude-oil spill site: I. Geochemical evolution of the plume. *J. Contam. Hydrol.* **2001**, *53*, 369−385.

(34) Thornton, S. F.; Lerner, D. N.; Banwart, S. A. Assessing the natural attenuation of organic contaminants in aquifers using plume-scale electron and carbon balances: model development with analysis of uncertainty and parameter sensitivity. *J. Contam. Hydrol.* **2001**, *53*, 199−232.

(35) Wiedemeier, T. H.; Rifai, H. S.; Newell, C. J.; Wilson, J. T. *Natural Attenuation of Fuels and Chlorinated Solvents in the Subsurface*; John Wiley & Sons: New York, 1997.

(36) Domenico, P. A. An analytical model for multidimensional transport of a decaying contaminant species. *J. Hydrol.* **1987**, *91*, 49−58.

(37) Aziz, C. E.; Newell, C. J.; Gonzales, J. R.; Haas, P. E.; Clement, T. P.; Sun, Y. BIOCHLOR natural attenuation decision support system: User's manual, version 1.1; U.S. EPA Office of Research and Development: Washington, DC, 2000.

(38) Newell, C. J.; McLeod, R. K.; Gonzales, J. BIOSCREEN Natural Attenuation Decision Support System; U.S. EPA Office of Research and Development: Washington DC, 1996.

(39) Borden, R. C.; Daniel, R. A.; LeBrun IV, L. E.; Davis, C. W. Intrinsic biodegradation of MTBE and BTEX in a gasoline-contaminated aquifer. *Water Resour. Res.* **1997**, *33*, 1105−1115.

(40) Tong, W.; Rong, Y. Estimation of methyl *tert*-butyl ether plume length using the Domenico analytical model. *Environ. Forensics* **2002**, *3*, 81−87.

(41) Stenback, G. A.; Kee Ong, S.; Rogers, S. W.; Kjartanson, B. H. Impact of transverse and longitudinal dispersion on first-order degradation rate constant estimation. *J. Contam. Hydrol.* **2004**, *73*, 3−14.

(42) Guyonnet, D.; Neville, C. Dimensionless analysis of two analytical solutions for 3-D solute transport in groundwater. *J. Contam. Hydrol.* **2004**, *75*, 141−153.

(43) Kuder, T.; Wilson, J. T.; Kaiser, P.; Kolhatkar, R.; Philp, P.; Allen, J. Enrichment of stable carbon and hydrogen isotopes during anaerobic biodegradation of MTBE: Microcosm and field evidence. *Environ. Sci. Technol.* **2005**, *39*, 213−220.

(44) Einarson, M. D.; Mackay, D. M. Predicting impacts of groundwater contamination-A new framework for prioritizing environmental site cleanups considers the interaction of contaminant plumes with water supply wells. *Environ. Sci. Technol.* **2001**, *35*, 66A−73A.

(45) Morasch, B.; Richnow, H. H.; Vieth, A.; Schink, B.; Meckenstock, R. U. Stable isotope fractionation caused by glycyl radical enzymes during bacterial degradation of aromatic compounds. *Appl. Environ. Microbiol.* **2004**, *70*, 2935−2940.

(46) Böckelmann, A.; Ptak, T.; Teutsch, G. An analytical quantification of mass fluxes and natural attenuation rate constants at a former gasworks site. *J. Contam. Hydrol.* **2001**, *53*, 429−453.

(47) Böckelmann, A.; Zamfirescu, D.; Ptak, T.; Grathwohl, P.; Teutsch, G. Quantification of mass fluxes and natural attenuation rates at an industrical site with a limited monitoring network: a case study. *J. Contam. Hydrol.* **2003**, *60*, 97−121.

(48) Herfort, M.; Ptak, T. Multitracer-Versuch im kontaminierten Grundwasser des Testfeldes Sud. *Grundwasser* **2002**, 31−40.

(49) Kjeldsen, P. Groundwater pollution source characterization of an old landfill. *J. Hydrol.* **1993**, *142*, 349−371.

(50) Mancini, S. A.; Ulrich, A. C.; Lacrampe-Couloume, G.; Slater, G. F.; Edwards, E. A.; Sherwood Lollar, B. Carbon and hydrogen isotopic fractionatin during anaerobic biodegradation of benzene. *Appl. Environ. Microbiol.* **2003**, *69*, 191−198.

(51) Meckenstock, R. U.; Morasch, B.; Warthmann, R.; Schink, B.; Annweiler, E.; Michaelis, W.; Richnow, H. H. $^{13}C/^{12}C$ stable isotope fractionation of aromatic hydrocarbons during microbial degradation. *Environ. Microbiol.* **1999**, *1*, 409−414.

(52) Morasch, B.; Richnow, H. H.; Schink, B.; Meckenstock, R. U. Stable hydrogen and carbon isotope fractionation during microbial toluene degradation: Mechanistic and environmental aspects. *Appl. Environ. Microbiol.* **2001**, *67*, 4842−4849.

(53) Christensen, T. H.; Bjerg, P. L.; Banwart, S. A.; Jakobsen, R.; Heron, G.; Albrechtsen, H. J. Characterization of redox conditions in groundwater contaminant plumes. *J. Contam. Hydrol.* **2000**, *45*, 165−241.

(54) Christensen, T. H.; Kjeldsen, P.; Bjerg, P. L.; Jensen, D. L.; Christensen, J. B.; Baun, A.; Albrechtsen, H. J.; Heron, G. Biogeochemistry of landfill leachate plumes. *Appl. Geochem.* **2001**, *16*, 659−718.

(55) Aelion, C. M. Impact of aquifer sediment grain size on petroleum hydrocarbon distribution and biodegradation. *J. Contam. Hydrol.* **1996**, *22*, 109−121.

(56) Garabedian, S. P.; LeBlanc, D. R.; Gelhar, L. W.; Celia, M. A. Large-scale natural gradient tracer test in sand and gravel, Cape Cod, Massachusetts, 2, Analysis of spatial moments for a nonreactive tracer. *Water Resour. Res.* **1991**, *27*, 911−924.

(57) LeBlanc, D. R.; Garabedian, S. P.; Hess, K. M.; Gelhar, L. W.; Quadri, R. D.; Stollenwerk, K. G.; Wood, W. W. Large-scale natural gradient tracer test in sand and gravel, Cape Cod, Massachusetts, 1, Experimental design and observed tracer movement. *Water Resour. Res.* **1991**, *27*, 895−910.